Unifying framework reveals importance of dissolved fluxes in ocean biological carbon pump

Mathieu A. Poupon[1,2*], Laure Resplandy[1,3] and Jessica Y. Luo[4]

[1*]Department of Geosciences, Princeton University, Princeton, 08544, NJ, USA.
[2]Atmospheric and Oceanic Sciences Program, Princeton University, Princeton, 08540, NJ, USA.
[3]High Meadows Environmental Institute, Princeton University, Princeton, 08544, NJ, USA.
[4]NOAA Geophysical Fluid Dynamics Laboratory, Princeton, 08540, NJ, USA.

*Corresponding author(s). E-mail(s): mpoupon@princeton.edu;
Contributing authors: laurer@princeton.edu; jessica.luo@noaa.gov ;

Abstract

The ocean biological carbon pump sequesters carbon from the atmosphere through diverse pathways, including gravitational settling, physical transport, and organism vertical migration. However, robust assessments of its magnitude remain challenging. Traditional approaches treat individual pathways separately, risking double counting fluxes when combining estimates, fail to capture the full range of spatio-temporal scales involved (from kilometers to thousands, hours to years), and focus on particulate carbon while overlooking dissolved fluxes. Here, we apply a unified framework quantifying all pathways simultaneously to a high-resolution (3 km) idealized model of the North Atlantic resolving seasonal, physical, and biological dynamics across scales, from regional biomes to fine-scale fronts. We show that carbon sequestration is dominated by the gravitational pump (∼70%), followed by physical (17–25%) and migrant (5–10%) pumps. Remarkably, carbon sequestration by the physical and migrant pumps is driven by dissolved fluxes—dissolved organic carbon transport and zooplankton respiration—which together account for over 20% of biological pump sequestration. Our findings underscore how unresolved dissolved fluxes and spatio-temporal variability —particularly physical pump fine-scale variability— can bias current estimates of the biological carbon pump, and call for a paradigm

shift toward integrative approaches combining next-generation observations with process-resolving models.

Keywords: Biological carbon pump, Dissolved fluxes, Ocean carbon cycle

1 Introduction

The ocean's biological carbon pump is a critical engine of the climate system, sequestering carbon away from the atmosphere [1, 2]. This sequestration occurs through a set of interconnected processes—referred to as 'pumps'—exporting and remineralizing both particulate and dissolved organic carbon in the ocean interior (Fig 1a,A1) [3]. Current estimates suggest these pumps export between 5 and 12 PgC yr^{-1} from the surface ocean [4–8] and sequester between 1100 and 1500 PgC in the ocean interior [8, 9]. However, none of these estimates fully capture all the pumps and their spatial and temporal scales, hindering our ability to accurately assess the biological carbon pump's current magnitude, its response to climate change, and role as a climate feedback – reinforcing or dampening of climate change by biological pump changes[10].

A comprehensive assessment of the biological pump requires disentangling intricate processes that export both particulate and dissolved organic carbon on different time and space scales. The gravitational pump is fueled by sinking particles (Fig 1b). The physical pumps transport both particulate and dissolved carbon through three mechanisms (Fig 1c): the large-scale pump transfers carbon via Ekman transport and overturning circulation [11], the mixed-layer pump exports carbon through seasonal mixed layer deepening and restratification [12, 13], and the eddy subduction pump through turbulent ocean dynamics, including fine-scale eddies and fronts ($<$ 200 km)[14, 15]. Finally, the migrant pump is powered by vertically migrating organisms, such as zooplankton, which actively transport particulate and dissolved carbon through egestion, excretion, and respiration along their migration path (Fig 1d) [16–18]. These pumps span a vast range of scales. Zooplankton migration occurs daily over hours and hundreds of meters [19], climate-driven circulation changes extend over decades and global scales [7, 20, 21], and in between, submesoscale fronts [14, 22] and mesoscale eddies [15, 23, 24] act on spatial scales of 1–100 km and temporal scales from days to months. This complexity and variability pose significant challenges for existing observational and modeling tools [25].

Current assessments remain limited by partial pump characterization and poor resolution of seasonal and fine-scale dynamics, leading to fragmented and incomplete estimates. Observational approaches often overlook dissolved carbon fluxes, which are

harder to measure than particulate fluxes [26, 27], and model studies rarely represent the migrant pump due to computational and conceptual trade-offs [7, 15, 20]. Typically, studies focus on a single pump at a time [26, 28–30], without isolating the contributions of other pumps, potentially causing double counting when aggregating individual estimates [3, 31]. Estimates are also constrained in spatio-temporal scales. Observations provide valuable snapshots in time and space but are challenging to extrapolate at regional and seasonal scales. Meanwhile, many global and regional models fail to resolve fine-scale processes such as eddies and fronts, playing a critical role in carbon export [15, 32]. Finally, while most studies focus on export fluxes, they rarely consider the depth at which this carbon is remineralized, which is key in determining its sequestration timescale in the interior ocean [2].

Here, we address these challenges by quantifying carbon export and sequestration across biological carbon pump components using a unifying framework applied to an idealized high-resolution model of the North Atlantic Ocean. This region covers contrasting biomes featuring marked seasonality and fine-scale dynamics [15, 32], and supports active gravitational, physical, and migrant carbon pumps [13, 16, 33, 34], offering a representative setting to understand their contribution to global carbon export and sequestration. The model explicitly resolves these three pumps and captures their spatio-temporal variability from hourly and kilometric scales to seasonal and regional scales. We show that the dissolved carbon fluxes control sequestration by physical and migrating pumps, and argue for increased attention to these fluxes in future biological carbon pump assessments. We show that the spatio-temporal variability in carbon pump export and the omission of dissolved fluxes can significantly bias previous estimates of the biological carbon pump.

2 Carbon flux contrasts in the North Atlantic

The high-resolution double gyre North Atlantic model reproduces the observed fine-scale and large-scale biophysical variability that structures the biological carbon pump, including primary productivity, zooplankton migrating biomass and vertical winter mixing (Fig 2, see details in Poupon et al. 2025 [35]). Specifically, the model captures the variability associated with turbulent dynamics, as shown by kilometric-scale chlorophyll filaments, reflecting fine-scale variations in primary productivity, and by eddy kinetic energy patterns, both matching satellite observations (Figs 2a-b, A2). The model also simulates the regional contrast between the high-productivity, high-seasonality subpolar biome (annual surface chlorophyll > 0.35 mg m^{-3}) and low-productivity, low-seasonality subtropical biome (annual surface chlorophyll < 0.15 mg m^{-3}, Fig 2c-d). In the subpolar biome, primary productivity peaks between May and June (0.92 gC m^{-2} d^{-1} in model and 0.65-0.93 gC m^{-2} d^{-1} in satellite, Fig 2e), followed by zooplankton migrating biomass that peaks between May and September (1.2 g m^{-2} in model and 1.4 g m^{-2} in observations, Fig 2g), with both reaching their minimum in winter (0.14 gC m^{-2} d^{-1} and 0.7 g m^{-2} in model, 0.10-0.24 gC m^{-2} and

d^{-1} and 0.4 g m^{-2} in satellite, Fig 2e,g). In contrast, in the subtropical biome, primary productivity and zooplankton migrant biomass remain relatively low and stable year-round (0.17-0.25 gC m^{-2} d^{-1} and 0.1-0.3 g m^{-2}, in both model and observations, Fig 2e,g). The model also captures the contrasting physical dynamics between the subpolar biome, where the mixed layer depth strongly varies from shallow summer (25-35 m) to deep winter (120-140 m) values, and the subtropical biome where it stays relatively shallow (30-60 m, Fig 2f).

These regional biophysical differences drive high carbon export and sequestration contrasts between subpolar and subtropical biomes. The simulated annual carbon export (defined as net carbon exported and remineralized below the euphotic zone, see Methods) in the high-productivity subpolar biome is 3 times greater than in the low-productivity subtropical biome (36 vs 12 gC m^{-2} yr^{-1}, Fig 3a, A3). This contrast is further amplified because, at any given remineralization depth, carbon remains sequestered for longer in the subpolar biome than in the subtropical biome (based on sequestration times from the Ocean Circulation Inverse Model [8], see Fig A4 and Methods). As a result, carbon sequestration is 3.6 times greater in the subpolar biome than in the subtropical biome (5.8 vs 1.6 kgC m^{-2}, Fig 3c). Despite these differences, we show in the following that relative contributions of the different pumps to export and sequestration, and the contribution of dissolved components are remarkably similar across biomes.

3 Carbon pump contributions to export and sequestration

The relative contributions of the gravitational, physical, and migrant pumps to carbon export and sequestration are similar across biomes (Fig. 3b). The gravitational pump dominates export (∼60% in both biomes), followed by the physical pumps (∼30%; mixed-layer: 10–12%, large-scale: 5–18%, eddy-subduction: 5–9%), and the migrant pump (∼10%; 6–11%). Pumps contributions to sequestration differ from export (Fig. 3b,d). The gravitational pump is highly efficient, with a contribution to sequestration that exceeds that of export (∼70% vs. ∼60%). In contrast, physical pumps are less efficient and contribute less to sequestration than to export (ranging from 17 to 25% across biomes; mixed-layer: 1 to 4%, large-scale: 2 to 20%, eddy-subduction: 5 to 10%). The migrant pump contributes similarly to both (5-10%, Fig. 3b,d).

These differences in pump efficiency are controlled by the depth at which carbon is exported and remineralized by each pump. The deeper the remineralization –via bacterial breakdown of POC and DOC or zooplankton respiration (see Methods) – the longer the carbon remains sequestered, and the more efficient the pump (Fig A4). Overall, most of the carbon sequestered by the biological pumps in the model is remineralized in the mesopelagic zone in both biomes (75% in upper 1000 meters, 50%

in upper 500 meters, Fig 4a-f), consistent with recent findings [36]. However, each pump injects remineralized carbon at distinct depths. In both biomes, the gravitational pump sustains most remineralization across the mesopelagic zone (upper 1000 m, Fig 4a,b). In contrast, the carbon exported by the physical pumps is mostly remineralized in the upper mesopelagic zone (above 300 m, Fig 4c,d), where downward ocean transport is most vigorous and accounts for 10–30% of total remineralization occurring at these depths (Fig 4g,h). Carbon exported by the migrant pump is mostly remineralized at migration depths (300–500 m, Fig. 4e,f), contributing 20–40% of remineralization there (Fig 4g,h). Thus, the physical pump is the least efficient due to its shallower remineralization depths, followed by the migrant pump, which supports remineralization only up to zooplankton migration depths, and finally the gravitational pump exporting over a deeper depth range.

4 Importance of dissolved carbon fluxes

Dissolved fluxes from the physical pump (DOC remineralization) and migrant pump (zooplankton respiration) support more than 20% of the total simulated carbon export and sequestration in the subpolar and subtropical biomes (gray bars in Fig 3c,d). The transport and remineralization of DOC contributes $\sim$ 62% to the physical pump sequestration (4% from the mixed layer pump, 19% from the eddy-subduction pump and 39% from the large scale pump), while POC only contributes $\sim$ 38% (Fig 3d and Fig A5). This large contribution of DOC to the physical pump sequestration is controlled by the different fate of exported DOC and POC in the water column. In fact, the physical pumps export more POC than DOC from the euphotic zone (14-19% vs 12-14% of total export, Fig 3c,d and FigA5), but POC is more rapidly remineralized ($\sim$hours to week) than DOC (days for labile DOC, months for semi-labile DOC, and decades for semi-refractory DOC), allowing DOC to be transported deeper by ocean currents before decomposition (Fig 4e,f). Specifically, remineralization of semi-refractory DOC accounts for most of the sequestration by the physical pump in the model (Fig A5) making it a key pathway of the biological carbon pump.

Contrary to the traditional view, the migrant pump sequesters carbon primarily through the injection of DIC via migrating zooplankton respiration. This injection of DIC by respiration accounts for 90% of the migrant pump carbon sequestration (Fig 3d, 4g,h). In contrast, POC egested by migrating zooplankton is largely confined to the euphotic zone (upper 100 m) and therefore contributes little to sequestration (Fig A6). This is mainly because digestion and egestion of POC by zooplankton occurs rapidly –within 15 minutes to 3 hours after feeding (Fig A7)– while zooplankton are still in the upper ocean. In contrast, zooplankton continuously respire [37, 38], injecting a larger amount of DIC at their migration depth ($\sim$300-500 m, Fig 4g,h) where they spent 9-17 hours during daytime (Fig. A7), leading to longer sequestration times for the injected DIC than for the egested POC (Fig 4e,f). Carbon sequestration by

dissolved components of the physical and migrant pumps exceeds that of their particulate components, at odds with the focus of previous studies quantifying these pumps [3, 26, 27].

5 Biological carbon pump spatio-temporal variability

The contribution of each pump to carbon export and sequestration vary significantly over time and space, even within biomes. Pump contributions exhibit strong seasonality in the subpolar biome, where biological and physical dynamics are marked by strong seasonal changes (Fig. 2e-g, 5a-b), while seasonality is much weaker in the subtropical biome (Fig. A8). The gravitational pump accounts for most of the subpolar seasonality (Fig. 5a) and follows the changes in organic particle production that peaks in spring – production of phytoplankton aggregates – and remains high in summer/-fall – production of fecal pellets and zooplankton carcasses (Fig. A9). Physical pumps exceed gravitational pump sequestration during winter and remain active through spring, summer and fall (Fig CC). The mixed-layer pump closely peaks in winter, following the deepening of the mixed layer (Fig. 5b, Fig 2f). The eddy subduction pump takes over in spring, when fine-scale dynamics restratifies the mixed layer [15, 39], and remains the main driver of the physical pump until the following winter (Fig. 5b). Carbon sequestration by the migrant pump peaks in summer (Fig. 5a), due to the combination of high zooplankton biomass, warmer temperatures enhancing metabolic rates, and longer day lengths causing zooplankton to spend more time at depth, all contributing to more respiration and carbon release at depth (Fig A7). As a result, the pumps sequester four times more carbon in spring than in winter.

The contribution of each pump also exhibits substantial spatial variability at fine-scale, potentially obscuring its mean influence on export. In the subpolar and subtropical biomes, the annual export is highly patchy, with variations within biomes rivaling the mean net export values (spatial standard deviation within each biome of 29 and 26 gC m^{-2} yr^{-1} compared to annual means of 36 and 12 gC m^{-2} yr^{-1}, Fig 3b). Most of this variability is attributable to the physical pumps (Fig 5a,A10), and more specifically the eddy subduction pump (Fig 5b). Fine-scale eddies and fronts drive intense and heterogeneous organic carbon fluxes on scales of a few kilometers (Fig 5d). However, downwards and upwards carbon export fluxes largely offset each other when averaged in space and time, resulting in a much smaller net flux at the biome scale and on average annually (Fig A11). Such variability in the physical pumps exists all year round and is concentrated within the top 500 meters (blue shading, Fig 4c,d), beneath which the intensity of the fine-scale dynamics decreases. Local estimates of carbon export and sequestration by the physical pumps are therefore unlikely to adequately represent their average values over a biome or on longer time scales. In contrast, the gravitational and migrant pumps are significantly less spatially variable (Fig 5a,c,e)

and their local measurements could be generalized more easily. This spatial and temporal variability complicates the quantification of each pump's contribution to carbon export and sequestration.

6 Toward new observational and modeling paradigms

These findings suggest paradigm shifts in understanding and quantifying the biological carbon pump. Historically, export and sequestration of particulate organic carbon have been easier to measure, using tools such as sediment traps [22] and backscattering sensors [26], and have thus received more attention [3]. However, dissolved fluxes remain difficult to measure and so far have been inferred by few observation- and model-based studies [11, 40–42], all focused on surface export, leaving the fate of deep DOC unresolved. Advancing our understanding of these dissolved components requires novel methodologies. For the migrant dissolved fluxes, global constraints such as zooplankton biomass, potentially measurable via LIDAR[43], and migration timing drivers need further exploration[44], alongside deeper investigations into mechanisms controlling metabolic rates (e.g., temperature[45], food availability[46] and internal cycles[47]). For the physical dissolved fluxes, more efficient methods to sample dissolved organic carbon and its lability are essential, complemented by studies into microbial processes that alter this lability[48, 49], often referred to as the "microbial pump"[50, 51].

Another major challenge in quantifying the biological carbon pumps lies in capturing their full spatio-temporal variability. We argue here that seasonal variations in pump contributions and the high spatial variability of physical pumps, with offsets between their downward and upward export fluxes, must be captured to constrain these pumps. Although float- and glider-based methods have been developed to measure the physical pumps at high spatio-temporal resolution [27, 52], they fail to capture the upward fluxes needed to evaluate these compensations, as well as their dissolved component. Previous studies have shown that small-scale atmospheric processes such as storms and cloud cover changes could also affect particle sinking [53] or migratory behavior [19]. This study does not represent these processes, nor physical processes smaller than 3 km, resulting in a potential underestimate of the biological carbon pump variability. Satellite methods show promising results for capturing fine-scale physical dynamics [54], phytoplankton ecosystem composition [55] and migrating biomass [43]. These direct approaches could be strategically complemented by biogeochemical tracer-based approaches integrating signals over time and filtering out variability [56, 57]. Overcoming these challenges is critical to improving our understanding of the biological carbon pump, constraining current estimates, and anticipating its response to future changes.

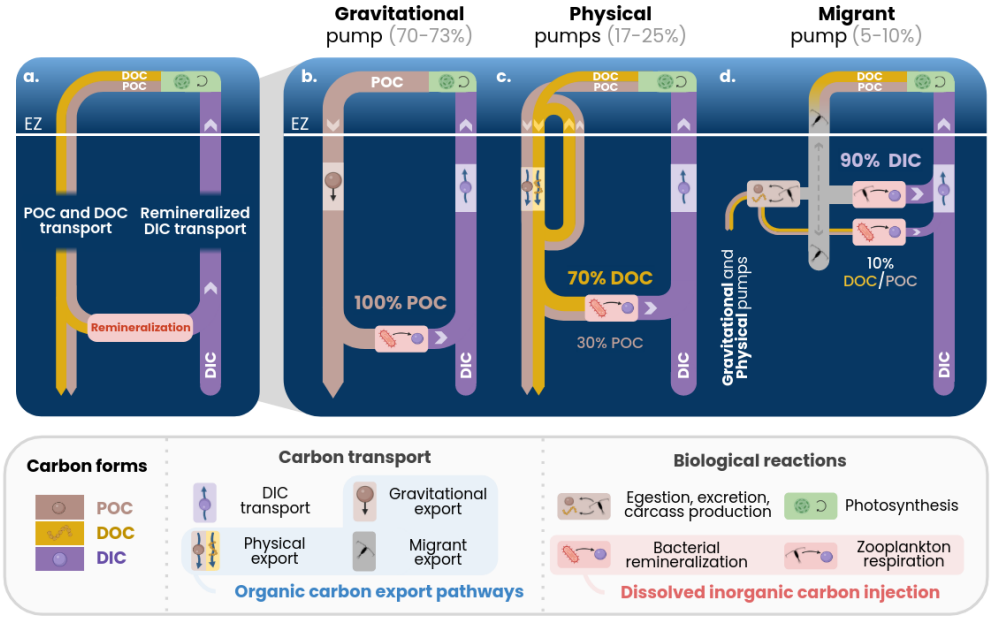

Fig. 1 (a) The biological carbon pump encompasses the (b) gravitational, (c) physical and (d) migrant pumps. These pumps act to increase the DIC gradient, via the production, export and remineralization of organic carbon, while the upward transport of remineralized DIC acts to decrease this gradient. Organic carbon is produced in dissolved and particulate form in the euphotic zone (EZ) through photosynthesis (green block), and is exported by the pumps. POC (brown) is transferred by gravitational settling, physical export, egestion of fecal pellets and the carcasses of migrating zooplankton. DOC (yellow) is transferred by the physical export and the excretion of migrating zooplankton. Remineralization of POC and DOC by bacteria and respiration by migrating zooplankton (red blocks) inject DIC (purple), which is sequestered in the interior ocean before being upwelled to the surface, closing the loop. Note that the arrow thickness is not conservative and proportional to the flux magnitudes.

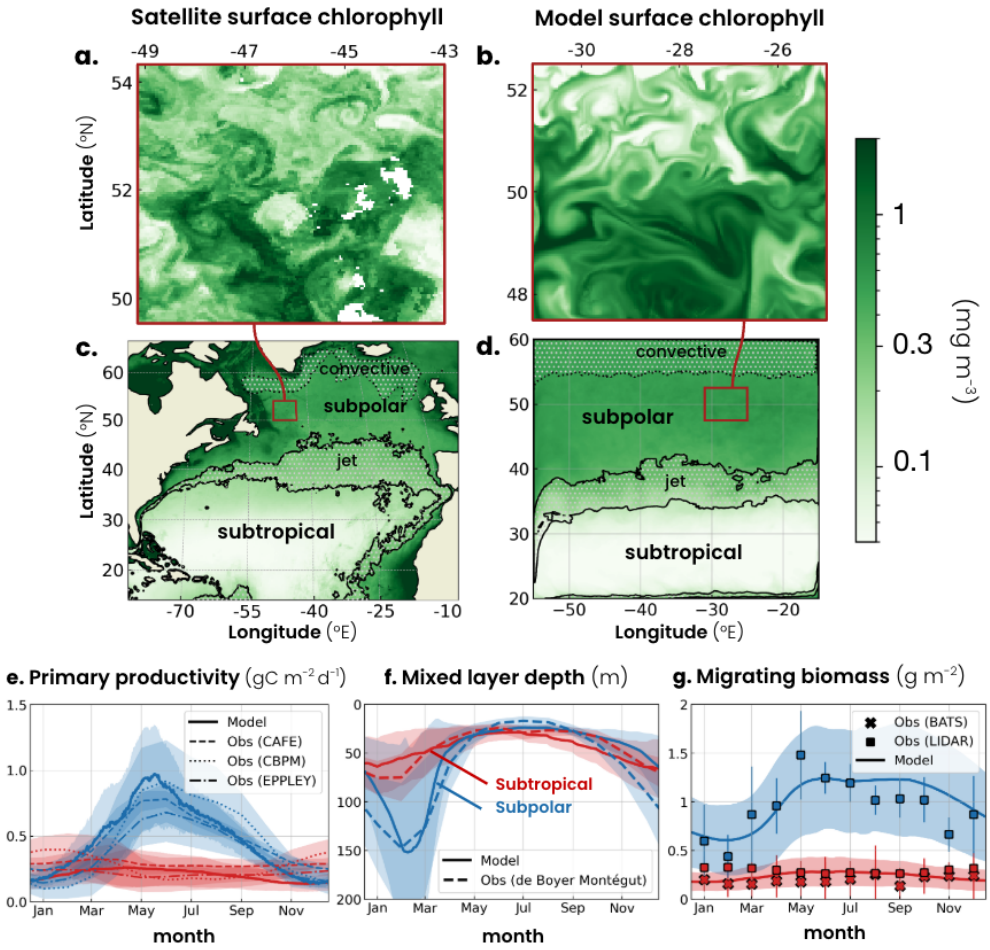

Fig. 2 Subpolar surface chlorophyll concentration snapshot from (a) satellite observations and (b) the double gyre model on March 10^{th}. Mean annual surface chlorophyll concentration from (c) satellite observations and (d) the double gyre model. Seasonal cycle of (e) net primary productivity, (f) mixed layer depth, and (g) migrating zooplankton biomass from observations (dotted lines) and in the model (solid lines). for the subpolar (blue) and subtropical (red) biomes. Shadings show the spatial variability within each biome (two standard deviations). Subtropical and subpolar biomes are defined by annual chlorophyll concentrations lower than 0.15 mg m^{-3} and higher than 0.35 mg m^{-3} respectively (black lines in a-b). Deep convection region defined by an annual mixed layer depth $>$ 150 m, and the jet region defined by chlorophyll concentrations between 0.15-0.35 mg m^{-3}, are excluded from the biome analysis (dotted areas in a-b). Sources of the observations are detailed in the method section.

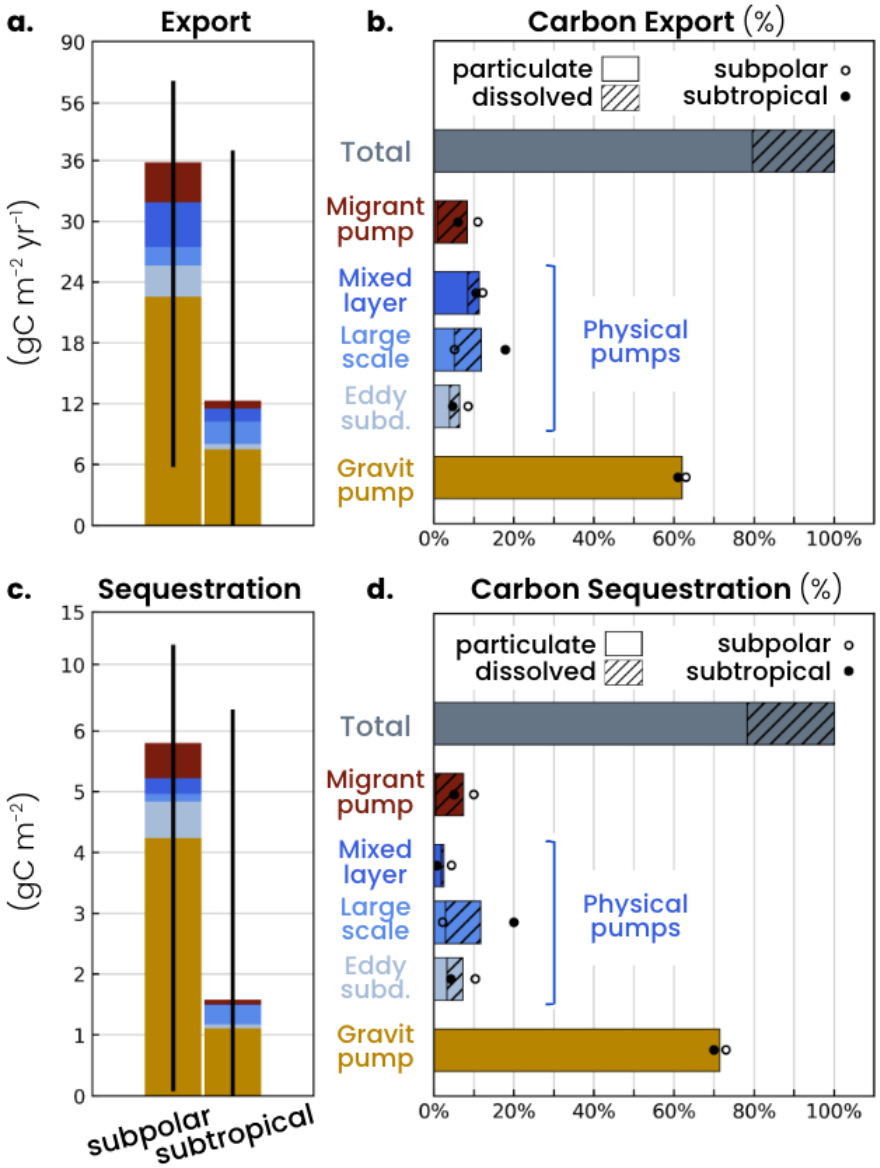

Fig. 3 (a) Annual carbon export and (c) carbon sequestration in the subpolar (left bars) and subtropical (right bars) biomes, partitioned among the gravitational (yellow), physical (blues), and migrant (red) pumps. The physical pumps include the mixed layer (dark blue), large-scale (blue), and eddy-subduction (light blue) pumps. Black lines indicate the annual spatial variability (± 1 standard deviation) within each biome. (b,d) Relative contributions of each pump to (b) carbon export and (d) sequestration across the model domain (excluding convective region; see Methods), using the same color scheme. Dashed bars represent dissolved carbon fluxes, and solid bars represent particulate fluxes. Hollow circles are the averages over the subpolar biome and filled circles over the subtropical biome.

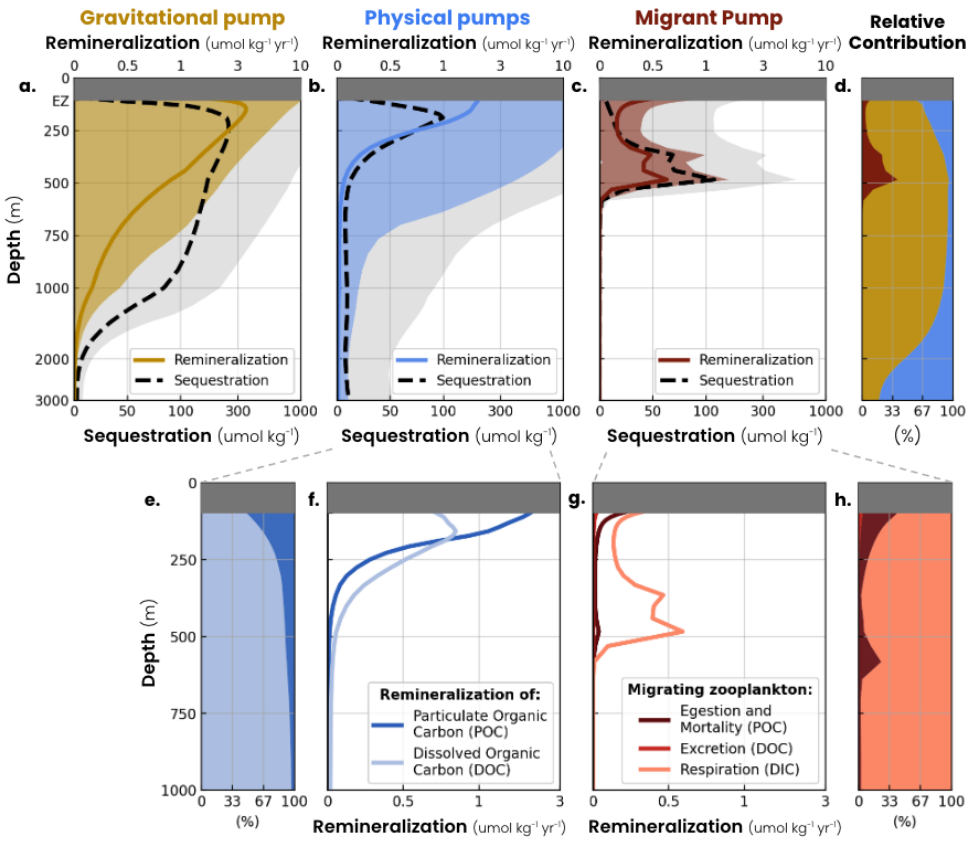

Fig. 4 (a-c) Vertical profiles of annual carbon remineralization rate (yellow, blue and red lines) and sequestration (dashed black lines) by the (a) gravitational, (c) physical and (e) migrant pumps. Shadings show the annual spatial variability (one standard deviations). (d) Vertical profiles of the mean relative contribution (in %) of the gravitational (yellow), physical (blue) and migrant (red) pumps to carbon remineralization rate and sequestration. (e-f) Vertical profile of the (e) relative and (f) absolute contribution of particulate organic carbon (dark blue) and dissolved organic carbon (light blue) remineralization to the physical pump. (g-h) Vertical profile of the (g) absolute and (h) relative contribution of migrating zooplankton respiration (light red, DIC production), excretion (red, DOC production), egestion and mortality (dark red, POC production) to the migrant pump. The annual mean euphotic zone (EZ, depth with 0.1% of surface irradiance) is masked out in grey.

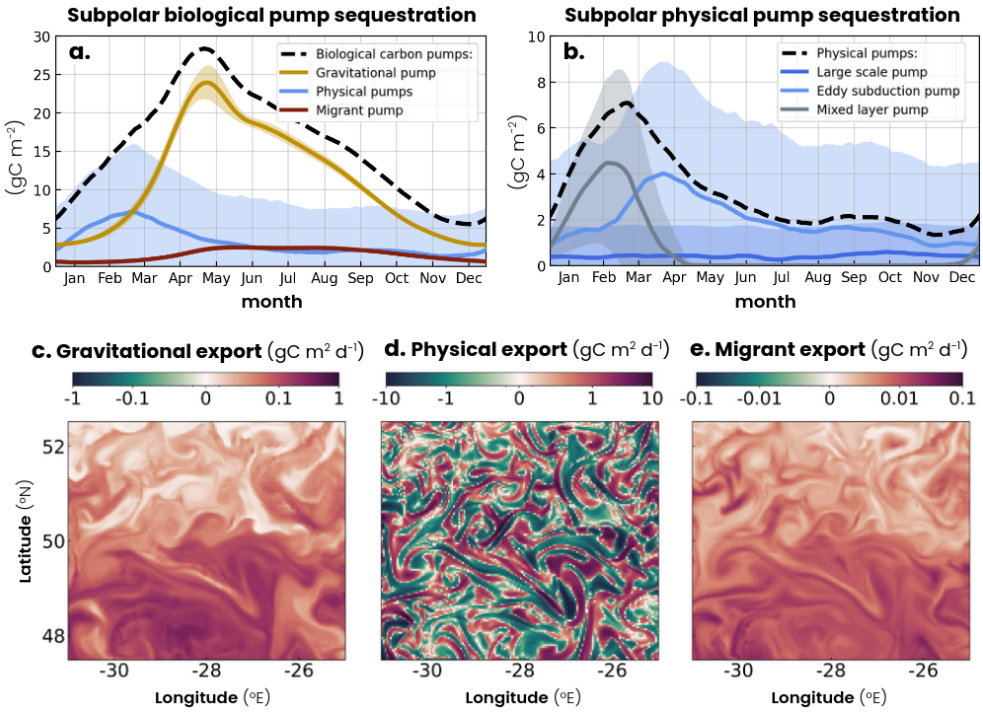

Fig. 5 (a) Seasonal cycle of carbon sequestration in the subpolar biome by the biological carbon pumps (dashed black), which is the sum of the gravitational (yellow), physical (blue) and migrant (red) pumps. (b) Seasonal cycle of carbon sequestration in the subpolar biome by the physical pumps (dashed black), which is the sum of the large scale (dark blue), the eddy subduction (light blue) and the mixed layer (grey) pumps. The shadings show the daily spatial variability of the pumps within the biome (two standard deviations). Snapshots of the carbon export by the (c) gravitational, (d) physical and (e) migrant pumps on March 10^{th} in the subpolar biome (-31°E to -25°E, 48.5°N to 52.5°N, same as Fig2a-b).

7 Methods

Model description

The study uses an idealized double gyre model reproducing the North Atlantic dynamics, described in Poupon et al. (2025)[35]. This model couples an ocean physical model (Modular Ocean Model version 6)[58], developed by the Geophysical Fluid Dynamics Laboratory, with a biogeochemical module detailed below. The model domain is a box 3570 km side length and 4 km deep, centred around 40°N. To better represent fine-scale dynamics, we increased the horizontal resolution from 9 km to 3 km compared to Poupon et al. (2025)[35], with updated model parameters available in supplementary (Table A1). This 3 km model is initialized from outputs of the 9 km model run for 100 years. The 3 km model is then spun-up for 25 years. The surface of the model is continuously forced by an idealized seasonal cycle, including a sinusoidal zonal wind profile inducing a double gyre circulation.

The physical model is coupled to the COBALTv2-DVM (Carbon, Ocean Biogeochemistry and Lower Trophics version 2 with Diel Vertical Migration) biogeochemical module [35, 59]. This module features 45 biogeochemical tracers, including the main nutrients (i.e. nitrogen, phosphorus, silica, and iron) and a planktonic ecosystem composed of 3 phytoplankton and 5 zooplankton, 3 non-migrating and 2 migrating. This module represents the dynamics of suspended particulate organic carbon, in the form of a planktonic ecosystem, sinking organic carbon in the form of detritus produced by phytoplankton aggregation or zooplankton egestion and mortality, dissolved inorganic carbon, and dissolved organic carbon (labile, semi-labile, and refractory). Labile dissolved organic carbon is remineralized over a few days, semi-labile over 90 days, and refractory over 10 years. The COBALTv2-DVM module also explicitly represents the diel vertical migration of zooplankton as well as their compartmentalized physiology that temporally and spatially decouples ingestion, digestion, respiration, and growth.

Model biomes

The model replicates the dynamics of a low-productivity, low-seasonality subtropical biome and a high-productivity, high-seasonality subpolar biome typical of the North Atlantic Ocean. The subtropical biome is defined by an annual mean surface chlorophyll concentration below 0.15 mg m^{-3}. The subpolar biome is defined by a mean chlorophyll concentration above 0.35 mg m^{-3} and a mean mixed layer depth below 200 meters, to exclude model regions where deep convection is too strong and representative of dynamics occurring in the Norwegian and Greenland seas (see Poupon et al. 2025[35]).

Observations and validation

To evaluate the spatial and temporal variability of the biogeochemical dynamics simulated by the double-gyre model, we use satellite, ship-based, and float observations. The mixed layer depth is calculated from hydrographic profiles collected between 1941 and 2022 [60], zooplankton migrating biomass from LIDAR measurements between 2007 and 2019 [43], and nets collected at the Bermuda Atlantic Time Series (BATS) station between 1994 and 2010 [61]. Net primary productivity estimates are produced by three algorithms (Eppley, CbPM, and CAFE) applied to Moderate-Resolution Imaging Spectroradiometer measurements between 2002 and 2023 [62–64]. POC profiles come from optical backscatter measurements collected by Biogeochemical-Argo floats between 2010 and 2021[65], DIC profiles from the GLODAPv2.2023 database [66], and DOC profiles from a GEOTRACES compilation of ship measurements ranging from 1994 to 2021 [67].

Framework description

Carbon remineralization and sequestration

In our model, the total organic carbon remineralization (gC m^{-3} yr^{-1}) which produces dissolved inorganic carbon is the sum to the remineralization of particulate and organic carbon by bacteria, and the respiration of migrating and non-migrating plankton:

$$\begin{aligned}\text{Remineralization}(z) = \quad & \text{POC remineralization}(z) + \text{DOC remineralization}(z) \\ & + \text{Biological respiration}(z)\end{aligned} \tag{1}$$

We derive carbon sequestration (gC m^{-3}) as the product of this remineralization rate and carbon sequestration time (yr) in subtropical and subpolar biomes from the Ocean Circulation Inverse Model (OCIM) [6]):

$$\text{Sequestration}(z) = \text{Remineralization}(z) \times \text{Sequestration time}(z) \tag{2}$$

The carbon export is the amount of carbon remineralized below the euphotic zone depth, defined as 0.1% of the photosynthetically active radiation at the surface [68]:

$$\text{Export}(z) = \int_{Bottom}^{Euphotic\ \ Depth} \text{Remineralization}(z)\mathrm{d}z \tag{3}$$

The amount of carbon sequestered in the water column corresponds to the vertical integration of Sequestration(z).

Carbon export pathways

The contribution of export pathways (gravitational, physical, migrant) to carbon remineralization is calculated considering that their organic carbon supply balances the remineralization flux:

$$\text{Biological respiration} = \text{Migrant respiration} + \text{Non-Migrant respiration} \tag{4}$$

$$\begin{aligned}\text{POC remineralization} = &- w_g \frac{\partial POC}{\partial z} - \vec{v} \cdot \vec{\nabla} POC + K_H \nabla_H^2 POC \\ &+ \frac{\partial}{\partial z}\left(K_z \frac{\partial POC}{\partial z}\right) + \text{POC production} - \frac{\partial POC}{\partial t}\end{aligned} \tag{5}$$

$$\begin{aligned}\text{DOC remineralization} = &- \vec{v} \cdot \vec{\nabla} DOC + K_H \nabla_H^2 DOC \\ &+ \frac{\partial}{\partial z}\left(K_z \frac{\partial DOC}{\partial z}\right) + \text{DOC production} - \frac{\partial POC}{\partial t}\end{aligned} \tag{6}$$

DOC and POC are the concentrations of dissolved and particulate organic carbon, $v = (u, v, w)$ is the fluid velocity, wg is the gravitational sink velocity relative to the fluid, K_H and K_z are the horizontal and vertical diffusion coefficients. POC and DOC are produced by both migrating and non-migrating animals (egestion, excretion, mortality). Below the euphotic zone, production by non-migrant animals is marginal and can be neglected. On an annual average, the gyre is close to equilibrium. As a result, dDOC/dt and dPOC/dt are also marginal and can be neglected. Thus, the carbon remineralization equation (1) can be written:

$$\begin{aligned}\text{Remineralization}(z) = &\ \text{Gravitational pathway}(z) + \text{Physical pathway}(z) \\ &+ \text{Migrant pathway}(z)\end{aligned} \tag{7}$$

With:

$$\text{Gravitational pathway} = -w_g \frac{\partial POC}{\partial z} \tag{8}$$

$$\begin{aligned}\text{Physical pathway} = &- \vec{v} \cdot \vec{\nabla} POC + K_H \nabla_H^2 POC + \frac{\partial}{\partial z}\left(K_z \frac{\partial POC}{\partial z}\right) \\ &- \vec{v} \cdot \vec{\nabla} DOC + K_H \nabla_H^2 DOC + \frac{\partial}{\partial z}\left(K_z \frac{\partial DOC}{\partial z}\right)\end{aligned} \tag{9}$$

$$\text{Migrant pathway} = \text{Migrant respiration} + \text{Migrant POC and DOC production} \quad (10)$$

Physical pathway decomposition

The physical export pathway encompasses transport by large-scale circulation such as Ekman transport or overturning circulation (large-scale pathway), subduction induced by finescale structures such as sub-mesoscale fronts and mesoscale eddies (eddy subduction pathway), and transport induced by mixed layer deepening and restratification (mixed layer pathway).

$$\begin{aligned}\text{Physical pathway} = \quad & \text{Large scale pathway} + \text{Eddy-subduction pathway} \\ & + \text{Mixed layer pathway}\end{aligned} \quad (11)$$

We isolate the small and large advective components using a Reynold's decomposition[69]:

$$\overline{C\vec{v}} = \overline{C}\ \overline{\vec{v}} + \overline{C'\vec{v}'} \quad (12)$$

Where (—) is a gaussian spatial mean operator with a radius of 100 km and ($'$) the small scale residual. We isolate the vertical mixing in the mixing layer from the mixing in the interior ocean using an indicator function ($Ind_{z<MLD}$), which takes the value 1 for depths within the mixed layer and 0 otherwise, and vice versa for ($Ind_{z>MLD}$). This way, the three pathways of the physical pump are:

$$\begin{aligned}\text{Large scale pathway} = & -\vec{\nabla}\cdot\left(\overline{\vec{v}}\ \overline{POC} + \overline{\vec{v}}\ \overline{DOC}\right) + K_H\nabla_H^2\left(POC + DOC\right) \\ & + \frac{\partial}{\partial z}\left(K_z\left(\frac{\partial POC}{\partial z} + \frac{\partial DOC}{\partial z}\right)\right) \times Ind_{z>MLD}\end{aligned} \quad (13)$$

$$\text{Eddy subduction pathway} = -\vec{\nabla}\cdot\left(\overline{\vec{v}'POC'} + \overline{\vec{v}'DOC'}\right) \quad (14)$$

$$\text{Mixed layer pathway} = \frac{\partial}{\partial z}\left(K_z\left(\frac{\partial POC}{\partial z} + \frac{\partial DOC}{\partial z}\right)\right) \times Ind_{z<MLD} \quad (15)$$

This framework makes it possible to quantify not only the various components of the biological carbon pump, but also their respective spatial and temporal variability across all space and time scales.

Acknowledgements. We thank Gaby Negrete-Garcia for conducting the Geophysical Fluid Dynamics Laboratory internal review.

Declarations

Funding. The study has been supported by the National Science Foundation (Eddy effects on Biological Pump award number 2023108).

Competing interest. The authors declare no competing interests.

Data and Code availability. The COBALTv2-DVM model and idealized double gyre configuration presented in this paper are available on github at https://github.com/mpoupon/MOM6_Double_Gyre.

Author contribution. Conceptualization: MP, LR, JL. Data curation: MP. Formal analysis: MP. Funding acquisition: LR, JL. Investigation: MP. Methodology: MP. Software: MP. Supervision: LR, JL. Visualization: MP. Writing – original draft: MP. Writing – review and editing: MP, LR, JL.

Appendix A

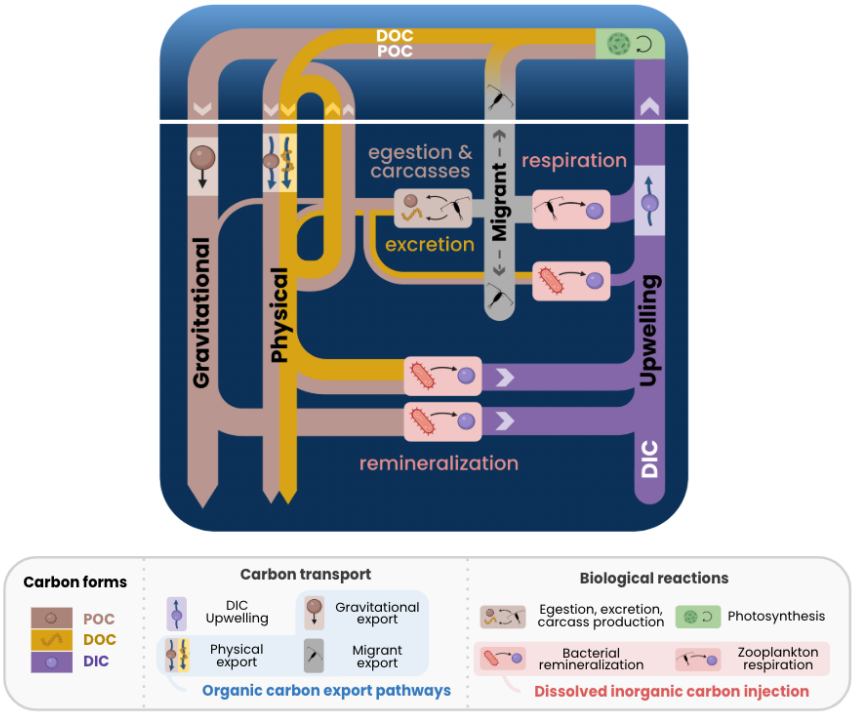

Fig. A1 Interconnection of the biological carbon pumps. Dissolved and particulate organic carbon is produced in the euphotic zone after photosynthesis (green block). The gravitational pump exports carbon out of the euphotic zone (white line) via gravitational settling. The physical pumps export the particles and the dissolved carbon via oceanic transport. The migrant pump exports carbon via respiration, the production of particles by egestion (fecal pellets) or mortality (carcasses), and the production of dissolved organic carbon (excretion) by the zooplankton migrating below the euphotic zone. The particles produced can then be exported deeper by the gravitational and physical pumps, while the dissolved organic carbon can be transported by the physical pump. This export sustains remineralization and injects DIC into the mesopelagic zone. The DIC from remineralization is sequestered in the interior ocean before being brought back to the surface by oceanic transport.

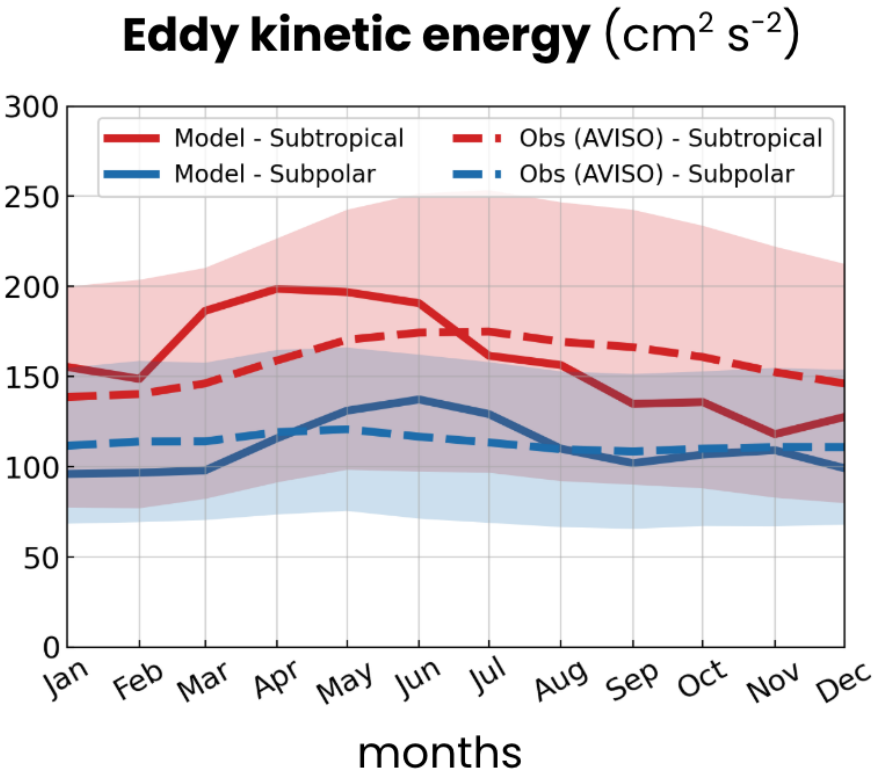

Fig. A2 Seasonal cycle of observed (dashed lines AVISO product) and modeled (solid lines) eddy kinetic energy in the subtropical (red) and subpolar (blue) biome. Shading represents the spatial variability of monthly values within the biomes (one standard deviation).

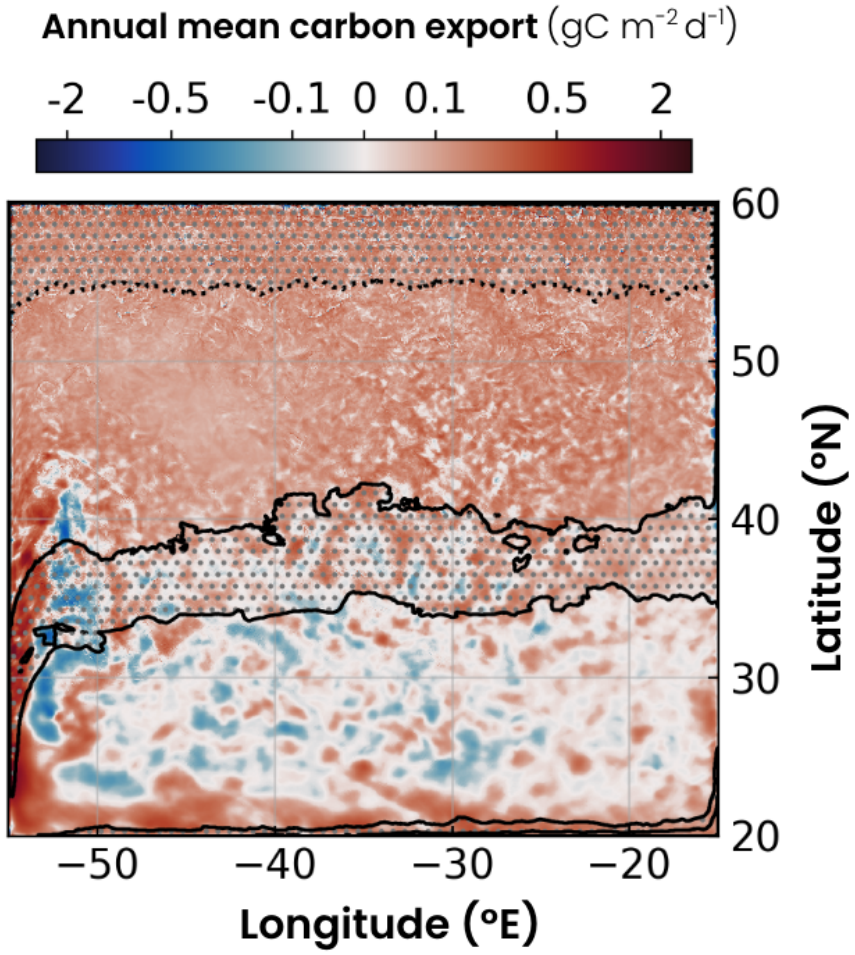

Fig. A3 Biological carbon export annual average in the double gyre model. Subtropical and subpolar biomes are defined by annual chlorophyll concentrations lower than 0.15 mg m-3 and higher than 0.35 mg m-3 respectively (black lines). Deep convection (∼55-60°N) region defined by an annual mixed layer depth ¿ 150 m, and the jet region (∼35-40°N) defined by chlorophyll concentrations between 0.15-0.35 mg m-3, are excluded from the biome analysis (dotted areas).

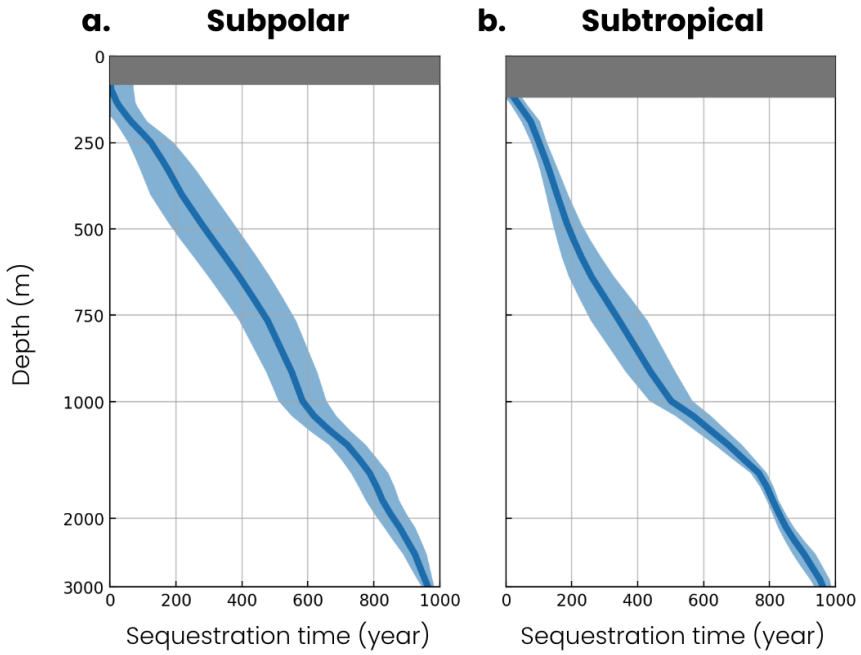

Fig. A4 Vertical profile of remineralized carbon sequestration time in the interior ocean in (a) the subpolar biome and (b) the subtropical biome from the OCIM model [6]. The fillings show the annual spatial variability of each pump within the biomes (two standard deviations). Grey boxes are the mean euphotic zone (EZ) extending down to the depth where irradiance is 0.1% of surface irradiance: 85m in the subpolar biome and 115 m in the subtropical biome.

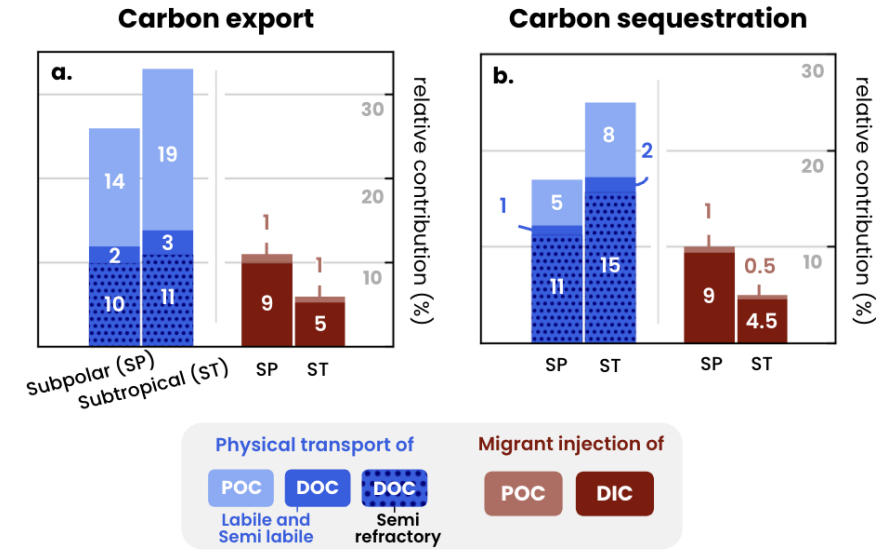

Fig. A5 Relative contribution of dissolved and particulate fluxes to (a) carbon export and (b) carbon sequestration by physical (blue) and migrant (red) pumps. Physical pumps export and sequester particulate carbon (light blue), labile and semi-labile dissolved carbon (dark blue) and semi-recalcitrant carbon (dark blue to point). The migrating pump exports and sequesters particulate carbon produced by the egestion or death of zooplankton (light red) as well as the respiration of zooplankton migrating along its migration trajectory (dark red).

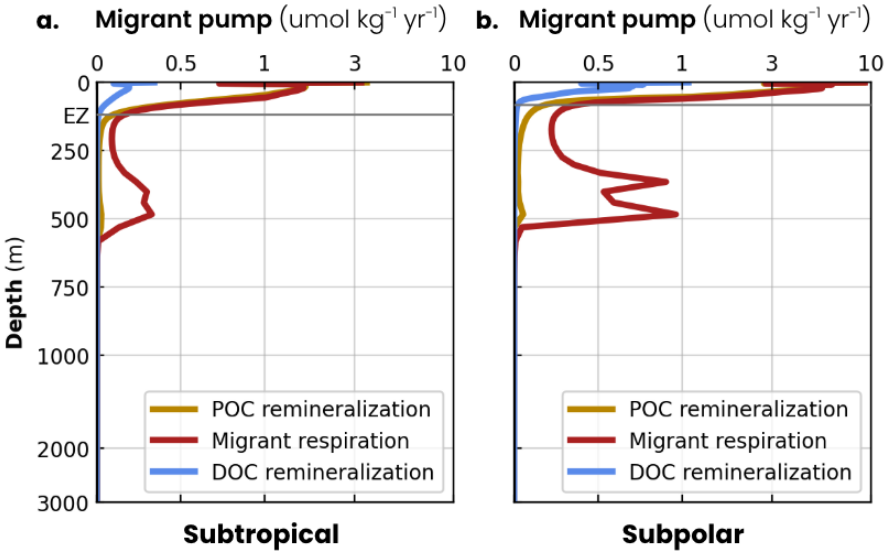

Fig. A6 Average annual vertical profile of remineralized carbon by the migrant pump in (a) subtropical and (b) subpolar biomes. Remineralization is supported by the production of organic particles (e.g., particle or carcass management, brown line), DOC production (excretion, blue line), and respiration by migrant zooplankton (red line). The euphotic zone (EZ) boundary in both biomes is represented by a horizontal gray line.

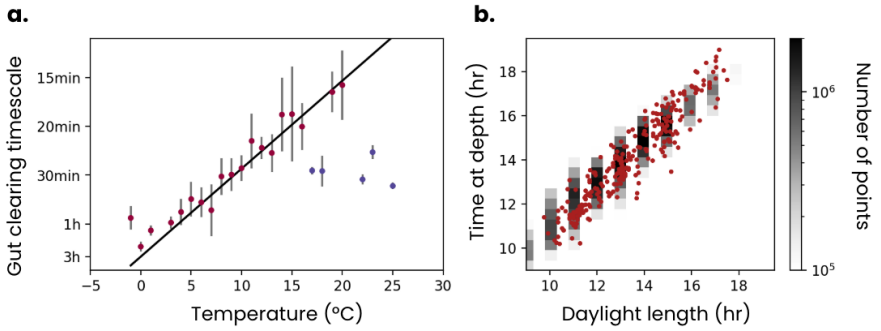

Fig. A7 (a) Time scale of gut clearance observed by Irigoien ([70], dots) and modeled in the COBALTv2-DVM model (black line) as a function of temperature. Observations are binned by degree of temperature and the gray lines represent a standard deviation. (b) Time spent at depth by migrating zooplankton as a function of the duration of daylight in the model (black shading) and the observation-based data product compiled by Bianchi et al. (2016[71], red dots).

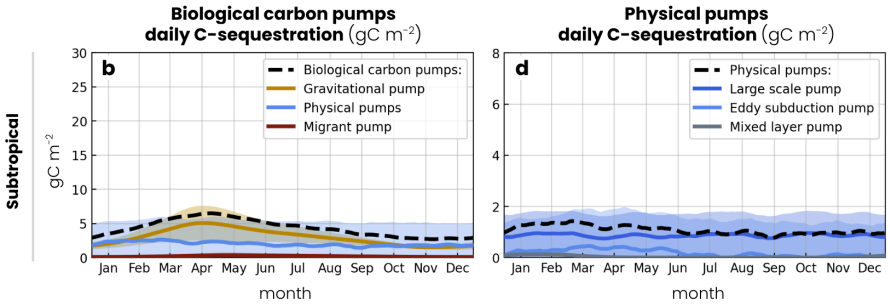

Fig. A8 (a) Seasonal cycle of carbon sequestration in the subtropical biome by the biological carbon pumps (dashed black), which is the sum of the gravitational (yellow), physical (blue) and migrant (red) pumps. (b) Seasonal cycle of carbon sequestration in the subpolar biome by the physical pumps (dashed black), which is the sum of the large scale (dark blue), the eddy subduction (light blue) and the mixed layer (grey) pumps. The shadings show the daily spatial variability of the pumps within the biome (two standard deviations).

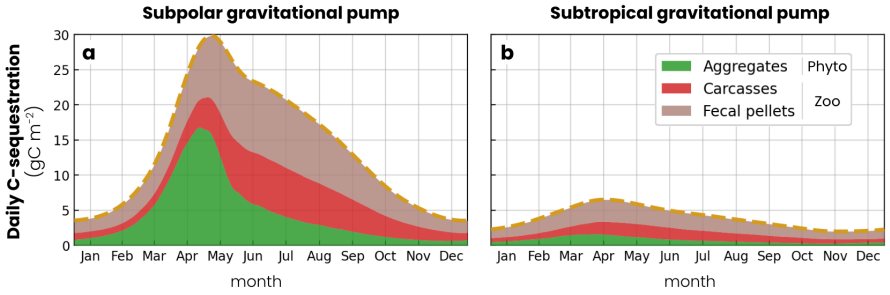

Fig. A9 Seasonal cycle of carbon sequestration by the gravitational pump in the (a) subpolar and (b) subtropical biome (black dotted lines). Sinking particles originate from phytoplankton aggregation (green), zooplankton caracasses (red) and zooplankton fecal pellets (orange).

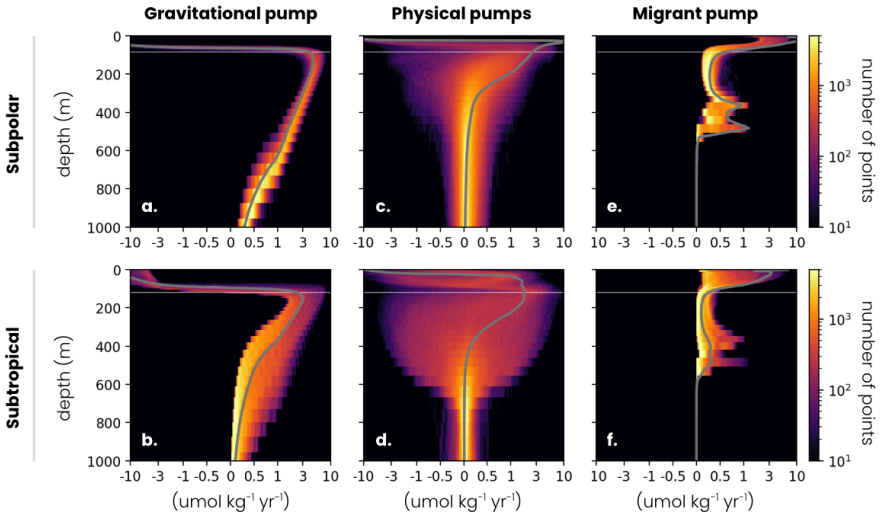

Fig. A10 Annual carbon remineralization vertical distribution in (top row) the subpolar biome and (bottom row) the subtropical biome by (a,b) the gravitational pump, (c,d) the physical pumps and (e,f) the migrant pump. The gray lines is the annual average value.

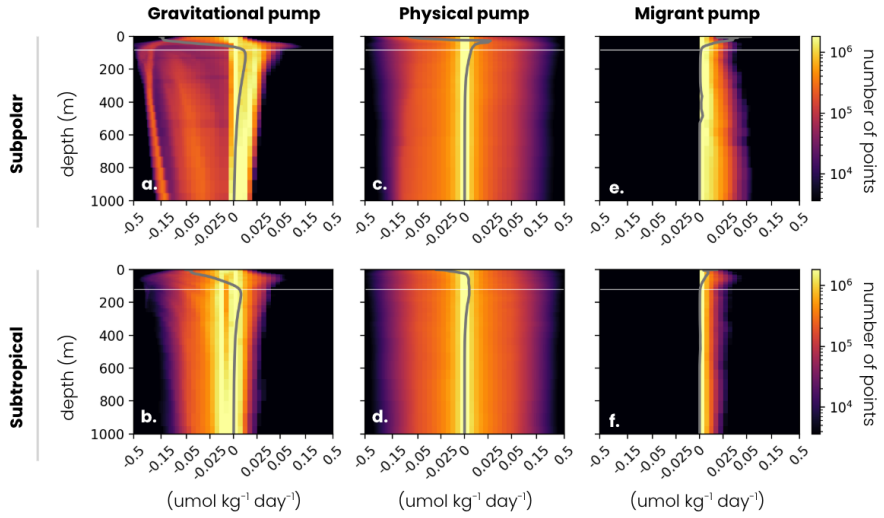

Fig. A11 Daily carbon remineralization vertical distribution in (top row) the subpolar biome and (bottom row) the subtropical biome by (a,b) the gravitational pump, (c,d) the physical pumps and (e,f) the migrant pump. The gray lines is the annual average value.

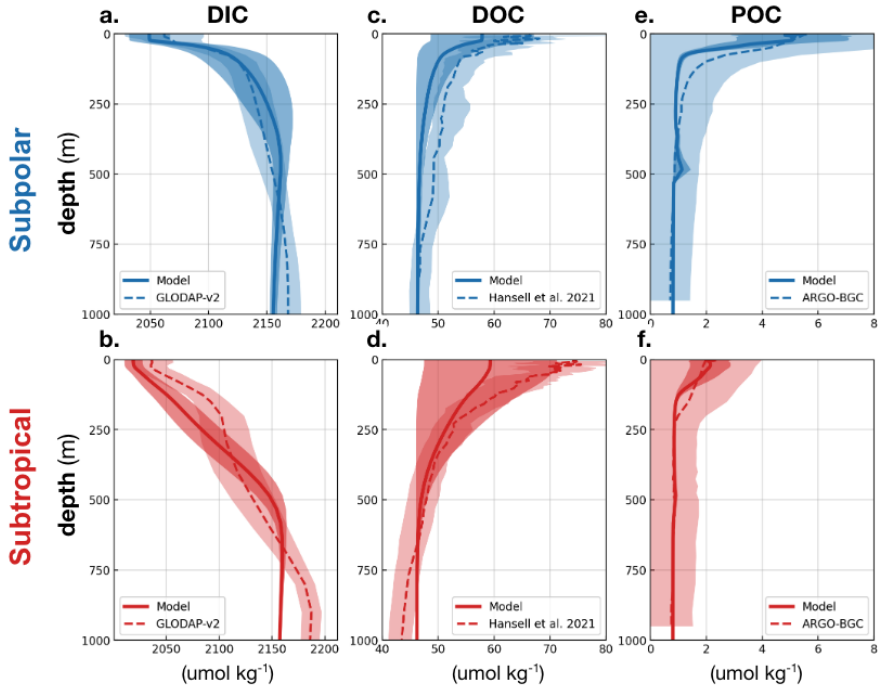

Fig. A12 Vertical profiles of annual (a,b) dissolved inorganic carbon, (c,d) dissolved organic carbon and (e,f) particulate organic carbon concentrations (dotted line) observed and (solid line) modeled in (a,c,e) the subpolar biome and (b,d,f) the subtropical biome. Shading is the spatial variability of this annual average within the biome (one standard deviation).

Table A1 Major parameters and associated values used in the physical ocean component of the model

Parameter	Values	References
Horizontal grid and resolution	1082 x 1082, 3.1 km	
Vertical coordinate	75 layer hybrid z*-isopycnal	(Adcroft et al. 2019)
Number of CPUs	1024	
Baroclinic and Biogeochemical time steps	100 s, 300 s	
Planetary boundary layer parameterization	ePBL	(Reichl and Hallberg. 2018)
Subgrid Mesoscale EKE parameterization	No	(Hallberg et al. 2013)
Submesoscale restratification parameterization	Frontal length = 1500 m	(Fox-Kemper et al. 2008)
Background kinematic viscosity	K_V=10^{-6} $m^2.s^{-1}$	
Background diapycnal diffusivity	K_D=10^{-6} $m^2.s^{-1}$	
Horizontal viscosity	Smagorinsky biharmonic Smagorinsky coefficient = 0.015 Resolution-dependent = 0.01 Δ_x^3 m^4s^{-1}	(Griffies et al. 2000)
Opacity Scheme	3-band with chlorophyll	(Manizza et al. 2005)

References

[1] Volk, T., Hoffert, M.I.: Ocean Carbon Pumps: Analysis of Relative Strengths and Efficiencies in Ocean-Driven Atmospheric CO2 Changes. In: The Carbon Cycle and Atmospheric CO2: Natural Variations Archean to Present, pp. 99–110. American Geophysical Union (AGU), ??? (1985). https://doi.org/10.1029/GM032p0099 . _eprint: https://onlinelibrary.wiley.com/doi/pdf/10.1029/GM032p0099. https://onlinelibrary.wiley.com/doi/abs/10.1029/GM032p0099 Accessed 2024-10-29

[2] Siegel, D.A., DeVries, T., Cetinić, I., Bisson, K.M.: Quantifying the Ocean's Biological Pump and Its Carbon Cycle Impacts on Global Scales. Annual Review of Marine Science **15**(1), 329–356 (2023) https://doi.org/10.1146/annurev-marine-040722-115226 . _eprint: https://doi.org/10.1146/annurev-marine-040722-115226. Accessed 2023-04-20

[3] Boyd, P.W., Claustre, H., Levy, M., Siegel, D.A., Weber, T.: Multi-faceted particle pumps drive carbon sequestration in the ocean. Nature **568**(7752), 327–335 (2019) https://doi.org/10.1038/s41586-019-1098-2 . Number: 7752 Publisher: Nature Publishing Group. Accessed 2022-01-30

[4] Henson, S.A., Sanders, R., Madsen, E.: Global patterns in efficiency of particulate organic carbon export and transfer to the deep ocean. Global Biogeochemical Cycles **26**(1) (2012) https://doi.org/10.1029/2011GB004099 . _eprint: https://onlinelibrary.wiley.com/doi/pdf/10.1029/2011GB004099. Accessed 2023-04-20

[5] Bopp, L., Resplandy, L., Orr, J.C., Doney, S.C., Dunne, J.P., Gehlen, M., Halloran, P., Heinze, C., Ilyina, T., Séférian, R., Tjiputra, J., Vichi, M.: Multiple stressors of ocean ecosystems in the 21st century: projections with CMIP5 models. Biogeosciences **10**(10), 6225–6245 (2013) https://doi.org/10.5194/bg-10-6225-2013 . Publisher: Copernicus GmbH. Accessed 2022-10-16

[6] DeVries, T., Weber, T.: The export and fate of organic matter in the ocean: New constraints from combining satellite and oceanographic tracer observations. Global Biogeochemical Cycles **31**(3), 535–555 (2017) https://doi.org/10.1002/2016GB005551 . _eprint: https://onlinelibrary.wiley.com/doi/pdf/10.1002/2016GB005551. Accessed 2023-04-20

[7] Kwiatkowski, L., Torres, O., Bopp, L., Aumont, O., Chamberlain, M., Christian, J.R., Dunne, J.P., Gehlen, M., Ilyina, T., John, J.G., Lenton, A., Li, H., Lovenduski, N.S., Orr, J.C., Palmieri, J., Santana-Falcón, Y., Schwinger, J., Séférian, R., Stock, C.A., Tagliabue, A., Takano, Y., Tjiputra, J., Toyama, K., Tsujino, H., Watanabe, M., Yamamoto, A., Yool, A., Ziehn, T.: Twenty-first century ocean warming, acidification, deoxygenation, and upper-ocean nutrient

and primary production decline from CMIP6 model projections. Biogeosciences **17**(13), 3439–3470 (2020) https://doi.org/10.5194/bg-17-3439-2020 . Publisher: Copernicus GmbH. Accessed 2022-10-16

[8] Nowicki, M., DeVries, T., Siegel, D.A.: Quantifying the Carbon Export and Sequestration Pathways of the Ocean's Biological Carbon Pump. Global Biogeochemical Cycles **36**(3), 2021–007083 (2022) https://doi.org/10.1029/2021GB007083 . _eprint: https://onlinelibrary.wiley.com/doi/pdf/10.1029/2021GB007083. Accessed 2023-04-20

[9] Carter, B.R., Feely, R.A., Lauvset, S.K., Olsen, A., DeVries, T., Sonnerup, R.: Preformed Properties for Marine Organic Matter and Carbonate Mineral Cycling Quantification. Global Biogeochemical Cycles **35**(1), 2020–006623 (2021) https://doi.org/10.1029/2020GB006623 . _eprint: https://onlinelibrary.wiley.com/doi/pdf/10.1029/2020GB006623. Accessed 2024-11-25

[10] Henson, S.A., Laufkötter, C., Leung, S., Giering, S.L.C., Palevsky, H.I., Cavan, E.L.: Uncertain response of ocean biological carbon export in a changing world. Nature Geoscience **15**(4), 248–254 (2022) https://doi.org/10.1038/s41561-022-00927-0 . Number: 4 Publisher: Nature Publishing Group. Accessed 2023-04-25

[11] Levy, M., Bopp, L., Karleskind, P., Resplandy, L., Ethe, C., Pinsard, F.: Physical pathways for carbon transfers between the surface mixed layer and the ocean interior. Global Biogeochemical Cycles **27**(4), 1001–1012 (2013) https://doi.org/10.1002/gbc.20092 . _eprint: https://onlinelibrary.wiley.com/doi/pdf/10.1002/gbc.20092. Accessed 2022-08-22

[12] Gardner, W.D., Chung, S.P., Richardson, M.J., Walsh, I.D.: The oceanic mixed-layer pump. Deep Sea Research Part II: Topical Studies in Oceanography **42**(2), 757–775 (1995) https://doi.org/10.1016/0967-0645(95)00037-Q . Accessed 2025-04-11

[13] Dall'Olmo, G., Dingle, J., Polimene, L., Brewin, R.J.W., Claustre, H.: Substantial energy input to the mesopelagic ecosystem from the seasonal mixed-layer pump. Nature Geoscience **9**(11), 820–823 (2016) https://doi.org/10.1038/ngeo2818 . Number: 11 Publisher: Nature Publishing Group. Accessed 2023-04-21

[14] Omand, M.M., D'Asaro, E.A., Lee, C.M., Perry, M.J., Briggs, N., Cetinić, I., Mahadevan, A.: Eddy-driven subduction exports particulate organic carbon from the spring bloom. Science (2015) https://doi.org/10.1126/science.1260062 . Publisher: American Association for the Advancement of Science. Accessed 2022-01-30

[15] Resplandy, L., Lévy, M., McGillicuddy Jr., D.J.: Effects of Eddy-Driven Subduction on Ocean Biological Carbon Pump. Global Biogeochemical Cycles **33**(8), 1071–1084 (2019) https://doi.org/10.1029/2018GB006125 . _eprint: https://onlinelibrary.wiley.com/doi/pdf/10.1029/2018GB006125. Accessed 2023-04-20

[16] Steinberg, D.K., Carlson, C.A., Bates, N.R., Goldthwait, S.A., Madin, L.P., Michaels, A.F.: Zooplankton vertical migration and the active transport of dissolved organic and inorganic carbon in the Sargasso Sea. Deep Sea Research Part I: Oceanographic Research Papers **47**(1), 137–158 (2000) https://doi.org/10.1016/S0967-0637(99)00052-7 . Accessed 2023-04-21

[17] Aumont, O., Maury, O., Lefort, S., Bopp, L.: Evaluating the Potential Impacts of the Diurnal Vertical Migration by Marine Organisms on Marine Biogeochemistry. Global Biogeochemical Cycles **32**(11), 1622–1643 (2018) https://doi.org/10.1029/2018GB005886 . _eprint: https://onlinelibrary.wiley.com/doi/pdf/10.1029/2018GB005886. Accessed 2023-04-20

[18] Pinti, J., DeVries, T., Norin, T., Serra-Pompei, C., Proud, R., Siegel, D.A., Kiørboe, T., Petrik, C.M., Andersen, K.H., Brierley, A.S., Visser, A.W.: Model estimates of metazoans' contributions to the biological carbon pump. Biogeosciences **20**(5), 997–1009 (2023) https://doi.org/10.5194/bg-20-997-2023 . Publisher: Copernicus GmbH. Accessed 2024-11-09

[19] Omand, M.M., Steinberg, D.K., Stamieszkin, K.: Cloud shadows drive vertical migrations of deep-dwelling marine life. Proceedings of the National Academy of Sciences **118**(32), 2022977118 (2021) https://doi.org/10.1073/pnas.2022977118 . Publisher: Proceedings of the National Academy of Sciences. Accessed 2023-04-24

[20] Wilson, J.D., Andrews, O., Katavouta, A., Melo Viríssimo, F., Death, R.M., Adloff, M., Baker, C.A., Blackledge, B., Goldsworth, F.W., Kennedy-Asser, A.T., Liu, Q., Sieradzan, K.R., Vosper, E., Ying, R.: The biological carbon pump in CMIP6 models: 21st century trends and uncertainties. Proceedings of the National Academy of Sciences **119**(29), 2204369119 (2022) https://doi.org/10.1073/pnas.2204369119 . Publisher: Proceedings of the National Academy of Sciences. Accessed 2023-11-08

[21] Dunne, J.P.: Physical Mechanisms Driving Enhanced Carbon Sequestration by the Biological Pump Under Climate Warming. Global Biogeochemical Cycles **37**(11), 2023–007859 (2023) https://doi.org/10.1029/2023GB007859 . _eprint: https://onlinelibrary.wiley.com/doi/pdf/10.1029/2023GB007859. Accessed 2025-04-11

[22] Stukel, M.R., Aluwihare, L.I., Barbeau, K.A., Chekalyuk, A.M., Goericke, R., Miller, A.J., Ohman, M.D., Ruacho, A., Song, H., Stephens, B.M., Landry, M.R.: Mesoscale ocean fronts enhance carbon export due to gravitational sinking and

subduction. Proceedings of the National Academy of Sciences **114**(6), 1252–1257 (2017) https://doi.org/10.1073/pnas.1609435114 . Publisher: Proceedings of the National Academy of Sciences. Accessed 2023-04-20

[23] McGillicuddy, D.J., Anderson, L.A., Bates, N.R., Bibby, T., Buesseler, K.O., Carlson, C.A., Davis, C.S., Ewart, C., Falkowski, P.G., Goldthwait, S.A., Hansell, D.A., Jenkins, W.J., Johnson, R., Kosnyrev, V.K., Ledwell, J.R., Li, Q.P., Siegel, D.A., Steinberg, D.K.: Eddy/Wind Interactions Stimulate Extraordinary Mid-Ocean Plankton Blooms. Science **316**(5827), 1021–1026 (2007) https://doi.org/10.1126/science.1136256 . Publisher: American Association for the Advancement of Science. Accessed 2023-04-21

[24] Chelton, D.B., Gaube, P., Schlax, M.G., Early, J.J., Samelson, R.M.: The Influence of Nonlinear Mesoscale Eddies on Near-Surface Oceanic Chlorophyll. Science **334**(6054), 328–332 (2011) https://doi.org/10.1126/science.1208897 . Publisher: American Association for the Advancement of Science. Accessed 2025-04-11

[25] Claustre, H., Legendre, L., Boyd, P.W., Levy, M.: The Oceans' Biological Carbon Pumps: Framework for a Research Observational Community Approach. Frontiers in Marine Science **8** (2021). Accessed 2022-02-17

[26] Llort, J., Langlais, C., Matear, R., Moreau, S., Lenton, A., Strutton, P.G.: Evaluating Southern Ocean Carbon Eddy-Pump From Biogeochemical-Argo Floats. Journal of Geophysical Research: Oceans **123**(2), 971–984 (2018) https://doi.org/10.1002/2017JC012861 . _eprint: https://onlinelibrary.wiley.com/doi/pdf/10.1002/2017JC012861. Accessed 2022-01-31

[27] Lacour, L., Llort, J., Briggs, N., Strutton, P.G., Boyd, P.W.: Seasonality of downward carbon export in the Pacific Southern Ocean revealed by multi-year robotic observations. Nature Communications **14**(1), 1278 (2023) https://doi.org/10.1038/s41467-023-36954-7 . Number: 1 Publisher: Nature Publishing Group. Accessed 2023-12-15

[28] Estapa, M.L., Feen, M.L., Breves, E.: Direct Observations of Biological Carbon Export From Profiling Floats in the Subtropical North Atlantic. Global Biogeochemical Cycles **33**(3), 282–300 (2019) https://doi.org/10.1029/2018GB006098 . _eprint: https://onlinelibrary.wiley.com/doi/pdf/10.1029/2018GB006098. Accessed 2025-04-11

[29] Haëntjens, N., Della Penna, A., Briggs, N., Karp-Boss, L., Gaube, P., Claustre, H., Boss, E.: Detecting Mesopelagic Organisms Using Biogeochemical-Argo Floats. Geophysical Research Letters **47**(6), 2019–086088 (2020) https://doi.org/10.1029/2019GL086088 . _eprint: https://onlinelibrary.wiley.com/doi/pdf/10.1029/2019GL086088. Accessed 2024-08-19

[30] Lacour, L., Briggs, N., Claustre, H., Ardyna, M., Dall'Olmo, G.: The Intraseasonal Dynamics of the Mixed Layer Pump in the Subpolar North Atlantic Ocean: A Biogeochemical-Argo Float Approach. Global Biogeochemical Cycles **33**(3), 266–281 (2019) https://doi.org/10.1029/2018GB005997 . _eprint: https://onlinelibrary.wiley.com/doi/pdf/10.1029/2018GB005997. Accessed 2025-04-11

[31] Lacour, L., Llort, J., Briggs, N., Strutton, P., Boyd, P.: Multi-year robotic observations reveal the seasonality of downward carbon export pathways in the Southern Ocean. Technical report (January 2022). https://doi.org/10.21203/rs.3.rs-1006941/v1 . ISSN: 2693-5015 Type: article. https://www.researchsquare.com/article/rs-1006941/v1 Accessed 2022-01-31

[32] Lévy, M., Ferrari, R., Franks, P.J.S., Martin, A.P., Rivière, P.: Bringing physics to life at the submesoscale. Geophysical Research Letters **39**(14) (2012) https://doi.org/10.1029/2012GL052756 . _eprint: https://onlinelibrary.wiley.com/doi/pdf/10.1029/2012GL052756. Accessed 2022-08-22

[33] Henson, S., Le Moigne, F., Giering, S.: Drivers of Carbon Export Efficiency in the Global Ocean. Global Biogeochemical Cycles **33**(7), 891–903 (2019) https://doi.org/10.1029/2018GB006158 . _eprint: https://onlinelibrary.wiley.com/doi/pdf/10.1029/2018GB006158. Accessed 2025-04-11

[34] Johnson, A.R., Omand, M.M.: Evolution of a Subducted Carbon-Rich Filament on the Edge of the North Atlantic Gyre. Journal of Geophysical Research: Oceans **126**(2), 2020–016685 (2021) https://doi.org/10.1029/2020JC016685 . _eprint: https://onlinelibrary.wiley.com/doi/pdf/10.1029/2020JC016685. Accessed 2023-10-30

[35] Poupon, M.A., Resplandy, L., Garwood, J., Stock, C., Zadeh, N., Luo, J.Y.: Chlorophyll shading reduces zooplankton diel migration depth in a high-resolution physical–biogeochemical model. Ocean Science **21**(2), 851–875 (2025) https://doi.org/10.5194/os-21-851-2025 . Publisher: Copernicus GmbH. Accessed 2025-05-12

[36] Ricour, F., Guidi, L., Gehlen, M., DeVries, T., Legendre, L.: Century-scale carbon sequestration flux throughout the ocean by the biological pump. Nature Geoscience **16**(12), 1105–1113 (2023) https://doi.org/10.1038/s41561-023-01318-9 . Publisher: Nature Publishing Group. Accessed 2024-09-14

[37] Countryman, C.E., Steinberg, D.K., Burd, A.B.: Modelling the effects of copepod diel vertical migration and community structure on ocean carbon flux using an agent-based model. Ecological Modelling **470**, 110003 (2022) https://doi.org/10.1016/j.ecolmodel.2022.110003 . Accessed 2025-04-11

[38] Thibault, H., Ménard, F., Abitbol-Spangaro, J., Poggiale, J.-C., Martini, S.:

Modeling the contribution of micronekton diel vertical migrations to carbon export in the mesopelagic zone. EGUsphere, 1–30 (2024) https://doi.org/10.5194/egusphere-2024-2074 . Publisher: Copernicus GmbH. Accessed 2025-04-11

[39] Mahadevan, A., D'Asaro, E., Lee, C., Perry, M.J.: Eddy-Driven Stratification Initiates North Atlantic Spring Phytoplankton Blooms. Science **337**(6090), 54–58 (2012) https://doi.org/10.1126/science.1218740 . Publisher: American Association for the Advancement of Science. Accessed 2023-04-21

[40] Carlson, C.A., Ducklow, H.W., Michaels, A.F.: Annual flux of dissolved organic carbon from the euphotic zone in the northwestern Sargasso Sea. Nature **371**(6496), 405–408 (1994) https://doi.org/10.1038/371405a0 . Publisher: Nature Publishing Group. Accessed 2025-05-11

[41] Carlson, C.A., Hansell, D.A., Nelson, N.B., Siegel, D.A., Smethie, W.M., Khatiwala, S., Meyers, M.M., Halewood, E.: Dissolved organic carbon export and subsequent remineralization in the mesopelagic and bathypelagic realms of the North Atlantic basin. Deep Sea Research Part II: Topical Studies in Oceanography **57**(16), 1433–1445 (2010) https://doi.org/10.1016/j.dsr2.2010.02.013 . Accessed 2025-05-11

[42] Roshan, S., DeVries, T.: Efficient dissolved organic carbon production and export in the oligotrophic ocean. Nature Communications **8**(1), 2036 (2017) https://doi.org/10.1038/s41467-017-02227-3 . Publisher: Nature Publishing Group. Accessed 2025-04-07

[43] Behrenfeld, M.J., Gaube, P., Della Penna, A., O'Malley, R.T., Burt, W.J., Hu, Y., Bontempi, P.S., Steinberg, D.K., Boss, E.S., Siegel, D.A., Hostetler, C.A., Tortell, P.D., Doney, S.C.: Global satellite-observed daily vertical migrations of ocean animals. Nature **576**(7786), 257–261 (2019) https://doi.org/10.1038/s41586-019-1796-9 . Number: 7786 Publisher: Nature Publishing Group. Accessed 2022-07-27

[44] Bandara, K., Varpe, O., Wijewardene, L., Tverberg, V., Eiane, K.: Two hundred years of zooplankton vertical migration research. Biological Reviews **96**(4), 1547–1589 (2021) https://doi.org/10.1111/brv.12715 . _eprint: https://onlinelibrary.wiley.com/doi/pdf/10.1111/brv.12715. Accessed 2022-10-03

[45] De Juan, C., Traboni, C., Calbet, A., Saiz, E.: Metabolic balance of a marine neritic copepod under chronic and acute warming scenarios. Marine Environmental Research **203**, 106827 (2025) https://doi.org/10.1016/j.marenvres.2024.106827 . Accessed 2025-01-16

[46] Berger, C.A., Steinberg, D.K., Tarrant, A.M.: Nutritional condition drives spatial variation in physiology of Antarctic lipid-storing copepods. Ecology and Evolution **14**(9), 70210 (2024) https://doi.org/10.1002/ece3.70210 . _eprint:

https://onlinelibrary.wiley.com/doi/pdf/10.1002/ece3.70210. Accessed 2025-01-16

[47] Maas, A.E., Timmins-Schiffman, E., Tarrant, A.M., Nunn, B.L., Park, J., Blanco-Bercial, L.: Diel metabolic patterns revealed by in situ transcriptome and proteome in a vertically migratory copepod. Molecular Ecology **33**(6), 17284 (2024) https://doi.org/10.1111/mec.17284 . _eprint: https://onlinelibrary.wiley.com/doi/pdf/10.1111/mec.17284. Accessed 2025-01-16

[48] Zakem, E.J., Cael, B.B., Levine, N.M.: A unified theory for organic matter accumulation. Proceedings of the National Academy of Sciences **118**(6), 2016896118 (2021) https://doi.org/10.1073/pnas.2016896118 . Publisher: Proceedings of the National Academy of Sciences. Accessed 2023-04-20

[49] Nguyen, T.T.H., Zakem, E.J., Ebrahimi, A., Schwartzman, J., Caglar, T., Amarnath, K., Alcolombri, U., Peaudecerf, F.J., Hwa, T., Stocker, R., Cordero, O.X., Levine, N.M.: Microbes contribute to setting the ocean carbon flux by altering the fate of sinking particulates. Nature Communications **13**(1), 1657 (2022) https://doi.org/10.1038/s41467-022-29297-2 . Number: 1 Publisher: Nature Publishing Group. Accessed 2023-04-21

[50] Jiao, N., Herndl, G.J., Hansell, D.A., Benner, R., Kattner, G., Wilhelm, S.W., Kirchman, D.L., Weinbauer, M.G., Luo, T., Chen, F., Azam, F.: The microbial carbon pump and the oceanic recalcitrant dissolved organic matter pool. Nature Reviews Microbiology **9**(7), 555–555 (2011) https://doi.org/10.1038/nrmicro2386-c5 . Publisher: Nature Publishing Group. Accessed 2024-11-06

[51] Jiao, N., Luo, T., Chen, Q., Zhao, Z., Xiao, X., Liu, J., Jian, Z., Xie, S., Thomas, H., Herndl, G.J., Benner, R., Gonsior, M., Chen, F., Cai, W.-J., Robinson, C.: The microbial carbon pump and climate change. Nature Reviews Microbiology **22**(7), 408–419 (2024) https://doi.org/10.1038/s41579-024-01018-0 . Publisher: Nature Publishing Group. Accessed 2025-04-11

[52] Llort, J., Langlais, C., Moreau, S., Lenton, A., Boyd, P.W., Matear, R., Strutton, P.: Occurrence of subduction events across the Southern Ocean and its contribution to the biological carbon pump (2018) https://doi.org/10.13140/RG.2.2.33780.04489 . Publisher: Unpublished. Accessed 2022-01-31

[53] Romanelli, E., Giering, S.L.C., Estapa, M., Siegel, D.A., Passow, U.: Can intense storms affect sinking particle dynamics after the North Atlantic spring bloom? Limnology and Oceanography **69**(12), 2963–2974 (2024) https://doi.org/10.1002/lno.12723 . _eprint: https://onlinelibrary.wiley.com/doi/pdf/10.1002/lno.12723. Accessed 2025-01-13

[54] Zhang, Z., Miao, M., Qiu, B., Tian, J., Jing, Z., Chen, G., Chen, Z., Zhao, W.: Submesoscale Eddies Detected by SWOT and Moored

Observations in the Northwestern Pacific. Geophysical Research Letters **51**(15), 2024–110000 (2024) https://doi.org/10.1029/2024GL110000 . _eprint: https://onlinelibrary.wiley.com/doi/pdf/10.1029/2024GL110000. Accessed 2025-01-13

[55] Cetinić, I., Rousseaux, C.S., Carroll, I.T., Chase, A.P., Kramer, S.J., Werdell, P.J., Siegel, D.A., Dierssen, H.M., Catlett, D., Neeley, A., Soto Ramos, I.M., Wolny, J.L., Sadoff, N., Urquhart, E., Westberry, T.K., Stramski, D., Pahlevan, N., Seegers, B.N., Sirk, E., Lange, P.K., Vandermeulen, R.A., Graff, J.R., Allen, J.G., Gaube, P., McKinna, L.I.W., McKibben, S.M., Binding, C.E., Calzado, V.S., Sayers, M.: Phytoplankton composition from sPACE: Requirements, opportunities, and challenges. Remote Sensing of Environment **302**, 113964 (2024) https://doi.org/10.1016/j.rse.2023.113964 . Accessed 2025-01-13

[56] Keppler, L., Landschützer, P., Gruber, N., Lauvset, S.K., Stemmler, I.: Seasonal Carbon Dynamics in the Near-Global Ocean. Global Biogeochemical Cycles **34**(12), 2020–006571 (2020) https://doi.org/10.1029/2020GB006571 . _eprint: https://onlinelibrary.wiley.com/doi/pdf/10.1029/2020GB006571. Accessed 2025-01-13

[57] Yamaguchi, R., Kouketsu, S., Kosugi, N., Ishii, M.: Global upper ocean dissolved oxygen budget for constraining the biological carbon pump. Communications Earth & Environment **5**(1), 1–12 (2024) https://doi.org/10.1038/s43247-024-01886-7 . Publisher: Nature Publishing Group. Accessed 2025-01-13

[58] Adcroft, A., Anderson, W., Balaji, V., Blanton, C., Bushuk, M., Dufour, C.O., Dunne, J.P., Griffies, S.M., Hallberg, R., Harrison, M.J., Held, I.M., Jansen, M.F., John, J.G., Krasting, J.P., Langenhorst, A.R., Legg, S., Liang, Z., McHugh, C., Radhakrishnan, A., Reichl, B.G., Rosati, T., Samuels, B.L., Shao, A., Stouffer, R., Winton, M., Wittenberg, A.T., Xiang, B., Zadeh, N., Zhang, R.: The GFDL Global Ocean and Sea Ice Model OM4.0: Model Description and Simulation Features. Journal of Advances in Modeling Earth Systems **11**(10), 3167–3211 (2019) https://doi.org/10.1029/2019MS001726 . _eprint: https://onlinelibrary.wiley.com/doi/pdf/10.1029/2019MS001726. Accessed 2022-10-16

[59] Stock, C.A., Dunne, J.P., Fan, S., Ginoux, P., John, J., Krasting, J.P., Laufkötter, C., Paulot, F., Zadeh, N.: Ocean Biogeochemistry in GFDL's Earth System Model 4.1 and Its Response to Increasing Atmospheric CO2. Journal of Advances in Modeling Earth Systems **12**(10), 2019–002043 (2020) https://doi.org/10.1029/2019MS002043 . _eprint: https://onlinelibrary.wiley.com/doi/pdf/10.1029/2019MS002043. Accessed 2022-10-16

[60] De Boyer Montégut, C.: Mixed layer depth climatology computed with a density threshold criterion of 0.03kg/m3 from 10 m depth value. SEANOE

(2023). https://doi.org/10.17882/91774 . https://www.seanoe.org/data/00806/91774/ Accessed 2024-12-03

[61] Steinberg, D.K., Lomas, M.W., Cope, J.S.: Long-term increase in mesozooplankton biomass in the Sargasso Sea: Linkage to climate and implications for food web dynamics and biogeochemical cycling. Global Biogeochemical Cycles **26**(1) (2012) https://doi.org/10.1029/2010GB004026 . _eprint: https://onlinelibrary.wiley.com/doi/pdf/10.1029/2010GB004026. Accessed 2023-12-06

[62] Behrenfeld, M.J., Falkowski, P.G.: A consumer's guide to phytoplankton primary productivity models. Limnology and Oceanography **42**(7), 1479–1491 (1997) https://doi.org/10.4319/lo.1997.42.7.1479 . Accessed 2024-06-19

[63] Westberry, T., Behrenfeld, M.J., Siegel, D.A., Boss, E.: Carbon-based primary productivity modeling with vertically resolved photoacclimation. Global Biogeochemical Cycles **22**(2), 2007–003078 (2008) https://doi.org/10.1029/2007GB003078 . Accessed 2024-06-19

[64] Silsbe, G.M., Behrenfeld, M.J., Halsey, K.H., Milligan, A.J., Westberry, T.K.: The CAFE model: A net production model for global ocean phytoplankton. Global Biogeochemical Cycles **30**(12), 1756–1777 (2016) https://doi.org/10.1002/2016GB005521 . Accessed 2024-06-19

[65] Dall'Olmo, G., Bhaskar TVS, U., Bittig, H., Boss, E., Brewster, J., Claustre, H., Donnelly, M., Maurer, T., Nicholson, D., Paba, V., Plant, J., Poteau, A., Sauzède, R., Schallenberg, C., Schmechtig, C., Schmid, C., Xing, X.: Real-time quality control of optical backscattering data from Biogeochemical-Argo floats. Open Research Europe **2**, 118 (2023) https://doi.org/10.12688/openreseurope.15047.2 . Accessed 2024-08-19

[66] Lauvset, S.K., Lange, N., Tanhua, T., Bittig, H.C., Olsen, A., Kozyr, A., Álvarez, M., Azetsu-Scott, K., Brown, P.J., Carter, B.R., Cunha, L., Hoppema, M., Humphreys, M.P., Ishii, M., Jeansson, E., Murata, A., Müller, J.D., Pérez, F.F., Schirnick, C., Steinfeldt, R., Suzuki, T., Ulfsbo, A., Velo, A., Woosley, R.J., Key, R.M.: The annual update GLODAPv2.2023: the global interior ocean biogeochemical data product. Earth System Science Data **16**(4), 2047–2072 (2024) https://doi.org/10.5194/essd-16-2047-2024 . Publisher: Copernicus GmbH. Accessed 2025-04-11

[67] Hansell, D.A., Carlson, C.A., Amon, R.M.W., Álvarez-Salgado, X.A., Yamashita, Y., Romera-Castillo, C., Bif, M.B.: Compilation of dissolved organic matter (DOM) data obtained from global ocean observations from 1994 to 2021. Version 2 (NCEI Accession 0227166). NOAA National Centers for Environmental Information (2021). https://doi.org/10.25921/S4F4-YE35 . https://www.ncei.noaa.gov/archive/accession/0227166 Accessed 2024-12-03

[68] Buesseler, K.O., Boyd, P.W., Black, E.E., Siegel, D.A.: Metrics that matter for assessing the ocean biological carbon pump. Proceedings of the National Academy of Sciences **117**(18), 9679–9687 (2020) https://doi.org/10.1073/pnas.1918114117 . Publisher: Proceedings of the National Academy of Sciences. Accessed 2023-10-13

[69] Levy, M., Couespel, D., Haeck, C., Keerthi, M.G., Mangolte, I., Prend, C.J.: Impact of finescale currents on biogeochemical cycles in a changing ocean. Annual Review of Marine Science (2023) https://doi.org/10.1146/((please . Accessed 2023-04-20

[70] Irigoien, X.: Gut clearance rate constant, temperature and initial gut contents: a review. Journal of Plankton Research **20**(5), 997–1003 (1998) https://doi.org/10.1093/plankt/20.5.997 . Accessed 2024-04-01

[71] Bianchi, D., Mislan, K.a.S.: Global patterns of diel vertical migration times and velocities from acoustic data. Limnology and Oceanography **61**(1), 353–364 (2016) https://doi.org/10.1002/lno.10219 . _eprint: https://onlinelibrary.wiley.com/doi/pdf/10.1002/lno.10219. Accessed 2023-04-20